

# Development of a Rapidly Deployable, Low-Cost Network of Hail Impact Disdrometers

Ian M. Giammanco

*Insurance Institute for Business & Home Safety*

Conrad J.P. Estes

*Insurance Institute for Business & Home Safety*

W. Edwin Cranford

*Insurance Institute for Business & Home Safety*

## 1. INTRODUCTION

Hailstorms represent the largest percentage of loss from the hazards associated with severe convective storms. They have also shown an increasing trend over the past decade (Changnon 2009; MunichRe 2014). The large damage potential of hailstorms has led to an increasing awareness and need to properly detect and mitigate the effect of hail. In addition, the emergence of convective allowing numerical weather prediction models and the recent upgrade of the National Weather Service's WSR-88D network to dual-polarimetric capability has provided new tools to help forecast, detect, and understand the spatial and temporal characteristics of hail at the ground. In order to improve hail forecasting and detection methods detailed observations of hail at the ground are needed. This is also vital for ensuring vulnerability curves for hazard damage modeling are accurate. While focus is often placed on the maximum hail size, the true damage potential of a hail event is a function of the hail size spectra at a given storm-relative location and aspects of the impacted material (e.g. type, age etc.). There remains a need to observe hail size distributions and how they evolve with time.

The majority of the historical literature examining hail size distributions employs data collected from hailpads. Hailpads are effective in obtaining bulk size distributions, they lack any information on the temporal characteristics of hail. They also require significant manpower to maintain, and can become saturated during events with very high concentrations of hail (Schleusener *et al.* 1960; Joss and Waldvogel 1967; Long *et al.* 1980). To alleviate the issues associated with conventional hailpads, automated sensors were developed to record both rain drop and hail sizes (Joss and Waldvogel 1967; Salmi *et al.* 2005; Lane *et al.*

2006). These systems typically rely on acoustic impact detection on a plate (Joss and Waldvogel 1967; Salmi *et al.* 2005; Lane *et al.* 2006). The impact induces a voltage output from the piezo-electric disk that can be measured. The signal properties of the impulse are related to the properties of the particle (i.e., energy, hardness). Other systems apply photogrammetric techniques to determine terminal velocities and size spectra (Schonhuber *et al.* 2008). Research in this arena has led to the commercial instrument systems with these abilities. However, the available units are often costly (>\$5,000) and may not be sufficiently rugged to survive repeated exposure to large hail events.

The emergence of low cost, open-source microcontrollers has opened the door to more cost-effective solutions for use in sampling hail. In addition, the success of adaptive, in-situ observing networks such as that described in Weiss and Schroeder (2008) and used during VORTEX 2 (Wurman *et al.* 2012) argued that this strategy could be applied toward hail research. This study presents the concept, design, and pilot deployment of a network of hail impact disdrometers. The platform integrates open-source "maker" components in order to provide a cost-effective detector for the sampling of hail.

## 2. CONCEPT AND DESIGN

The system design criteria focused on purely hail sampling with the ability of the system to be rapidly deployed. The deployment criteria is necessary so an array of probes can be set down in advance of an approaching thunderstorm and allow the deployment team to exit the path safely. The platform also must be able to withstand repeated impacts from large and even giant hail (> 10.16 cm).

## 2.1 Impact plate design and fabrication

Initially, two plate designs were fabricated and tested. The first followed the design used by Lane *et al.* (2006) which was a shallow four-sided pyramid with a single piezo-electric element. The second was a three-sided “delta” shape, intended to house three piezo-electric disks, one on each face. However, data acquisition and signal processing concerns rendered this design too complex. The plate design used by Lane *et al.* (2006), shown in Figure 1, was selected for use due to its simplicity and ability to shed water while not allowing hail to accumulate on its surface. The surface of the impact plate is 1 ft<sup>2</sup> (929 cm<sup>2</sup>) and is fabricated from 0.25 inch (0.635 cm) aluminum. As shown in Figure 1, the piezo-electric disk is mounted to a flat surface underneath the impact plate which is welded to each of the four sides. This allows the response of an impact on any of the sides to be transferred to the sensor (Lane *et al.* 2006). The full impact plate is then attached to an enclosure underneath which houses the data acquisition controller and internal battery.

## 2.2 Deployment platform

For rapid deployment, a small engineering tripod is used for the base of the probe, as shown in Figure 2. It is attached by a bolt which fits a threaded hole on the bottom of the enclosure. A bubble level is used to allow for leveling in the field using the adjustable legs on the tripod. The system can be easily configured for use in a fixed application through removing the mounting plate and attaching a pipe fitting flange (shown in Figure 1). Toggle switches control power and data functions. The instrument cable from the piezo-electric disk has a quick-disconnect so the impact plate assembly can be easily removed. Another connector on the outside of the enclosure allows for battery charging in the field or the use of an external power supply.

## 2.3 Signal characteristics and data acquisition

The impact of a particle on the plate will generate an electric response from the ceramic piezo-electric disk. The properties of the impact signal are related to the characteristics of the object striking it (e.g. size, mass, hardness,

etc.). Lane *et al.* (2006) modeled the response of the impact plate to a spring-mass-damper.

This allowed Lane *et al.* (2006) to use the peak amplitude of the impact signal to estimate the hydrometeor diameter and apply band-pass filter to distinguish between raindrops and hail impacts. The method required a minimum data acquisition (DAQ) sampling rate of 48 kHz (Lane *et al.* 2006). For typical research-grade DAQ systems this is easily achievable, however these systems are costly (> \$3000). To manage the cost of the platform, low-cost, commercially available microcontrollers were explored. These systems offer relatively fast processor speeds, support various communication protocols, and have versatile input/output configurations. The Arduino Due controller was found to be the most appropriate unit to serve as the data acquisition and processing platform for the probe. This was based on its 32-bit ARM CORE processor, 84 GHz clock, wide array of analog and digital input/outputs, and a unit cost of approximately \$50. A micro-SD module was added for on-board data storage as well as a GPS module for time and position information on a prototyping shield shown in Figure 3.

While the platform is quite powerful for its size and cost, during the initial development phase we were unable to produce consistently timed sampling faster than 5 kHz. An example of a raw 5 KHz time history from a detected hail impact is shown in Figure 4. This did not allow for the processing method of Lane *et al.* (2006) could not be used. The use of peak detection at this sampling rate produced too much variability. Instead, a post-processing approach was used and applied to the 5 KHz time history from the piezo-electric element. Impacts are identified by the rising signal voltage indicated by a positive  $\Delta V/\Delta t$  which is found using a centered difference approximation. Once the voltage change converges to zero, the impact signal is truncated and then operated on. The method similar to that used in acoustic raindrop detection by Joss and Waldvogel (1967), is applied. The technique applies the assumption that the integration of the signal curve in time is proportional to the kinetic energy of the object impacting the plate. A trapezoid approximation is used to calculate the integral by:

$$\int_a^b f(x)dx \approx \frac{h}{2} \sum_{k=1}^N f(x_{k+1}) + f(x_k) \quad (1)$$

where  $h$  represents the sampling interval in seconds and  $N$  is the number of samples contained in the impact packet.

### 3. CALIBRATION AND HAIL SIZE DETECTION

All acoustic disdrometers rely on relating the electronic impulse captured during a hydrometeor impact, to the force or energy that the object imparted on the plate. This is then related to the size of the object. The hail impact disdrometer presented here functions applying this model. In order to obtain useable information, laboratory impacts are used to obtain calibration curves.

#### 3.1 Calibration

The disdrometer probes are calibrated to impact kinetic energy through an empirical function. The calibration function for each probe was developed through impacting the platforms with ice spheres. The ice spheres were produced using a solution of distilled water and diffused carbon dioxide gas to produce a sphere with a mean density of  $0.8 \text{ g cm}^{-3}$  which is closer to that of natural hail (Giammanco *et al.* 2015). Nominal diameters of 2.54, 3.17, 3.81, 4.45, 5.08 cm were used. The spheres were pneumatically propelled at target kinetic energies based on Laurie (1960). The actual kinetic energy was calculated by measuring the velocity and the mass of each propelled sphere. Impacts were randomly distributed across the face of the probe in order to capture variability associated with inherent fabrication non-uniformities. A photograph of a calibration impact is shown in Figure 4. A least-squares power law curve was fitted to the relationship between the area under the impact signal packet and the known kinetic energy, an example is shown in Figure 3. Each probe was calibrated individually and the coefficients and goodness of fit for each of the 6 probes are shown in Table 1. Differences were found between the calibration functions and the fitted curves typically accounted for 80% of the variance. The 95% confidence interval yielded a mean uncertainty across all the six probes of  $\pm 0.25 \text{ V}$  in the integrated impact signal curve. This corresponds to a maximum instrument error of approximately  $\pm 1.5 \text{ J}$ . This is non-trivial when applied towards estimating hailstone sizes which have a range of kinetic energies for a given diameter. The error is mostly random as

a result of the sampling rate and the properties of the impact plate. It is noted that faster sampling could greatly reduce the error and will be explored in the future.

The discrimination between large rain drops and hail will plague any impact disdrometer. Testing of the probes in purely rain environments showed that some droplet impacts were captured. For deep convection, the melting of graupel and small hail can produce droplet sizes that approach 0.50 – 0.90 cm with similar kinetic energies to hailstones of similar diameters (Brandes *et al.* 2003; Zhang *et al.* 2009; Cao and Zhang 2009). While the signal properties of the two different hydrometeor impacts are different in the frequency domain, the 5 kHz sampling rate did not allow the discrimination technique of Lane *et al.* (2006) to be applied. This is a limitation of the system such that the true hail size spectra cannot be determined with precision. However, since these small hailstones ( $< 1.00 \text{ cm}$ ) are likely not damaging, for understanding the distribution of damaging hail and categorization the configuration of the system presented here is adequate. In the future, comparisons with Parsivel laser disdrometer measurements will help in understanding the droplet sizes the platform physically detects.

#### 3.2 Hail size estimation

The disdrometer impact probe is designed to detect the kinetic energy of falling hailstones but an estimate of hailstone size can be extracted through existing diameter – kinetic energy relationships. Recent work by Heymsfield *et al.* (2014) has provided equations to describe estimate hailstone diameter to kinetic energy relationships. Equation 2 represents the fitted curve for all hailstones that Heymsfield *et al.* (2014) examined, and can be applied to the impact kinetic energy captured by the probe. This relationship is described by:

$$KE = 0.037 D^{3.94} \quad (2)$$

where  $D$  is the hailstone diameter. This is based on improved estimates of Reynolds Number effects and aerodynamic drag presented in Heymsfield and Wright (2013). The post processing algorithm solves Equation 2 for the hailstone diameter using the detected kinetic energy. The results of Heymsfield *et al.* (2014) support that this method is purely an estimate and that in wind-driven conditions, hailstones

may exceed their theoretical terminal velocities producing large size errors. Using the pilot data collected in 2015, this estimate of hailstone sizes is investigated and compared with physical measurements of hail at probe deployment sites.

#### **4. 2015 FIELD DEPLOYMENT**

Six impact disdrometer probes were completed for use in 2015 during the Insurance Institute for Business & Home Safety's annual field measurement program (for a summary of this program please see Brown *et al.* 2014). During the 2015 campaign, 36 individual probe deployments were made on eight different parent thunderstorms. The successful deployments are summarized in Table 2. The strategy was to deploy an array of probes in advance of a hail producing thunderstorm along a selected roadway. Typical storm translation speeds required at least 40 minutes of lead time to deploy the array safely. Disdrometer probes were typically spaced 2.00 – 3.00 km apart according to the recommended observation spacing suggested by Long (1978) in an effort to capture the true hail mass within a thunderstorm. For supercell storm modes, the intersection of the updraft/mesocyclone and the deployment roadway was used to center the array. This ideally would sample both the forward flank and hook-echo regions. For non-supercell modes, the horizontal radar reflectivity maximum was targeted. Upon retrieval of the probes, physical measurements of hail were made within an approximate 5 m<sup>2</sup> area surrounding the probe to compare with estimated hailstone sizes.

##### **4.1 Comparisons with measured hail**

Field measurement teams were able to measure hail in the immediate vicinity of deployed probes in order to compare the hail size estimates with physical measurements. For the purposes of this study, we examine the estimated hail size from the disdrometer probe despite its relatively large potential error. It is also noted that hail distributions over small areas are quite random but this provided a measure of the general performance of the system. The estimated sizes detected by the disdrometer probes were larger than those measured in five of the eight successful deployments in which physical measurements

of hail were made, as shown in Figure 6. In two deployments, hail below 1 cm was detected but was not found by measurement teams following the passage of the targeted thunderstorm. The result was expected given some influence from melting prior to the field teams arriving at the deployment site. The mean difference between the measured maximum and the peak detected estimate was -0.32 cm. The absolute value of the difference yielded a mean difference of 1.04 cm. With the previously described sources of error, the results were encouraging, especially given the range of possible kinetic energies for specific hail diameters shown by Heymsfield *et al.* (2014). The median value of the measured hail distribution (measured, detected) was larger, likely as a result from the melting of small hail, contamination from large drops, and the inherent error associated with the impact plate and data processing system. The lack of any extreme outliers in the measured differences suggests that simultaneous impacts were negligible in these cases.

##### **4.2 8 May 2015 Supercell Case Study**

A discrete supercell was intercepted during the late afternoon on 8 May 2015 and all six disdrometer probes deployed in a north-south array between Dickens and Spur, TX. Operations on this day began in the morning with elevated convection. Two sub-arrays (3 probes each) were deployed for disorganized convection near Childress, TX. By late afternoon, surface-based convection developed east of Lubbock, TX and the dominant updraft quickly acquired supercell characteristics. The disdrometer deployment team began their deployment at approximately 2020 UTC along State Highway 70 north of Dicken, TX. Probes were spaced approximately 2 km apart. The southern-most disdrometer (Probe 106) was located approximately 1 km north of Spur, TX. The evolution of the target supercell as it approached the disdrometer array is shown in Figure 7. The supercell began to exhibit a deviant motion toward the southeast as it approached the array. This occurred while the deployment was in progress, resulting in the southern-most probe remaining north of the mesocyclone. By 2120 UTC the supercell had cleared the disdrometer array. During the deployment the supercell was tornado warned but no tornado was observed by the deployment team.

Three of the six probes (southern half of the array, Probes 104-106) detected impacts. The low-level reflectivity maximum associated with the supercell passed between probes 105 and 106. The KLBB 0.5° differential reflectivity ( $Z_{DR}$ ) indicated values near zero extending from near probe 105 southward past the probe 106 location for three consecutive volume scans. These were collocated with horizontal reflectivity values of 55 – 60 dBz which provides high confidence that hail was present. Probe 104 recorded three impacts while probes 105 and 106 recorded more substantial hail as shown in the time history of size concentrations in Figure 6. In this figure, estimated hail sizes are grouped into 1.00 cm bins using 10 second time windows. Hail was first detected by probe 105 at approximately 2044 UTC which was (at the time) outside the 50 dBz horizontal reflectivity contour but  $Z_{DR}$  values were near zero supporting the presence of hail. Probe 104 detected the three hail impacts from 2045 – 2048 UTC, two of which fell in the smallest size bin (< 1.00 cm / large drops) and one in the 1.00-2.00 cm group. Further south, Probe 105 indicated a nearly continuous presence of either small hail or large drops from 2044 – 2052 UTC, with peak concentrations in the smallest size group of 1 impact per second. The estimated maximum hail size captured by this probe was 2.00-3.00 cm with impacts also occurring in the 1.00-2.00 cm bin as well (Figure 6). The deployment team physically measured a hailstone of 2.80 cm (largest hailstone) at this location with an average size of 1.71 cm from the 17 hailstones measured. Further south, closer to the mesocyclone, Probe 106 first detected hail at 2047 UTC with larger impacts falling in the three bins from 2-5 cm between 2049 – 2052 UTC and maximum detected estimated size of 4.85 cm. A 4.10 cm hailstone was measured by the deployment team at this location when the probe was retrieved (see Figure 7, Probe 106) with a mean (median) of 2.26 cm (1.85 cm) for a sample size of 19. Concentrations peaked at 5 impacts per 10 seconds. Larger hailstones were measured 2-4 km south of probe 106, very near the mesocyclone track and within the hook echo region to the storm-relative right of the circulation path. This pattern of larger stones falling outside the “core” region (near the horizontal reflectivity maximum) was noted by Kumjian *et al.* (2014) and has been qualitatively observed for other supercell cases.

## 5. SUMMARY

The emergence of “maker” microcontroller systems led to the investigation of their use in developing a low-cost hail impact disdrometer. The impact plate design of Lane *et al.* (2006) was coupled with an Arduino Due to produce a low-cost hail impact disdrometer. The platform was also designed to be rapidly deployable such that a network of probes could be set down in an array ahead of a hail producing thunderstorm. Six probes were developed and successfully deployed for the first time in 2015. The deployment team was able to complete individual probe deployments often in less than one minute and safely exit the path of the approaching parent thunderstorm. The use of a larger number of probes could shrink the margin of error associated with storm motion changes without sacrificing deployment team safety.

The results from the 2015 field campaign showed that this platform can effectively capture and characterize hail impacts. However sampling limitations and the characteristics of natural hail limit its ability to function as a precision instrument. This will hold true for any impact disdrometer that relies on signal to impact kinetic energy relationships. The results of Heymsfield *et al.* (2014) support the notion that for a given natural hail diameter there is a range of possible kinetic energies which will limit the precision of any impact-based detector. Despite these limitations, the system is adequate for general hail size characterizations, kinetic energy distributions, and spatial analysis of hail through time to space conversions. These types of data are vital for correlating dual-polarimetric radar hail signatures as well as understanding the general size concentration which will influence the severity of damage. The total platform cost was approximately \$750 (hardware and fabrication) making this system very cost effective. The system will continue to be evaluated in 2016 in order to examine hail size distributions with respect to conventional hail pads and to understand the size of rain drops the platform resolves. The success of this low-cost system may also foster the development of automated building hail detection systems for more operational or event characterization applications.

## ACKNOWLEDGEMENTS

This work was supported by the Insurance Institute for Business & Home Safety and its member companies. The authors wish to thank Dr. Tanya Brown-Giammanco for her helpful insights and for handling logistics during the 2015 field campaign. We also thank Heather Sommers and Hank Pogorzelski for their tireless work in the field deploying probes to collect the information presented here.

## REFERENCES

- Brandes, E.A., G. Zhang, and J. Vivekanandan (2003), An evaluation of a drop distribution-based polarimetric radar rainfall estimator. *J. Appl. Meteor.*, **42**, 652-660.
- Brown, T.M., I.M. Giammanco, M.R. Kumjian, (2014), IBHS hail field research program 2012-2014. *AMS 27th Conference on Severe Local Storms*, Madison, WI.
- Heymsfield, A.J. and R.L. Wright, (2013), Graupel and hail terminal velocities: Does a supercritical Reynolds Number apply, *J. Atmos. Sci.*, **71**, 3392 – 3403.
- Heymsfield, A.J., I.M. Giammanco, and R.L. Wright, (2014) Terminal velocities and kinetic energies of natural hailstones, *Geo. Phys. Res. Lett.*, **41**. 8666-8672
- Joss, J. and A. Waldvogel, (1967), Ein spektrograph für Niederschlagstropfen mit automatischer Auswertung. *Pure Appl. Geophys.*, **68**, 240-246.
- Kumjian, M.R., T.M. Brown, and I.M. Giammanco, (2014) IBHS hail field project 2014 case studies: Comparisons of polarimetric radar observations and surface hail characteristics. *AMS 27th Conference on Severe Local Storms*, Madison, WI.
- Lane, J.E., R.C. Youngquist, W.D. Haskell, R.B. Cox, (2006), A Hail size impact transducer, *J. Acoust. Soc. Am.*, **119**, 47-53.
- Laurie, J. A. P. (1960), Hail and its effects on buildings, Council for Scientific and Industrial Research, Report No. 176, Pretoria, South Africa, 12 pp.
- Long, A.B., R.J. Matson and E.L. Crow, (1960), The hailpad: Materials, data reduction and calibration. *J. Appl. Meteor.*, **19**, 1300–1313.
- MunichRe (2014), 2013 Natural Catastrophe Review, MunichRe NatCat Services, Philadelphia, PA., <http://www.munichre.com/en/reinsurance/business/non-life/natcatservice/annual-statistics/index.html>.
- Salmi, A., and J. Ikonen, (2005), New piezoelectric Vaisala RAINCAP precipitation sensor. 19<sup>th</sup> Conf. of Hydrology, San Diego, *Amer. Meteor. Soc.*, P2.6.
- Schleusener, R.A., and P.C. Jennings, (1960), An energy method for relative estimates of hail intensity. *Bull. Am. Meteorol. Soc.* **41**, 372–376.
- Schönhuber, M., G. Lammer, and W. L. Randeu (2008), The 2D video disdrometer. Precipitation: Advances in measurement, estimation and prediction, S. Michaelides, Ed., Springer, 3–31.
- Weiss, C. C., and J. L. Schroeder, (2008), StickNet: A new portable rapidly deployable surface observations system, *Bull. Amer. Meteor. Soc.*, **89**, 1502-1503.
- Wurman J., D. Dowell, Y. Richardson, P. Markowski, Erik Rasmussen, D. Burgess, L. Wicker, and H.B. Bluestein, (2012). The second verification of the origins of rotation in tornadoes experiment: VORTEX2. *Bull. Amer. Meteor. Soc.*, **93**, 1147–1170.

Table 1. Least-squares fitted power-law calibration coefficients and goodness of fit for each disdrometer probe. Each uses a power law of the form:  $y = ax^b$  where  $y$  is kinetic energy and  $x$  is the area under the signal curve packet for an individual impact.

Probe	$a$	$b$	$R^2$
101	12.83	0.81	0.83
102	12.85	0.81	0.78
103	12.41	0.86	0.81
104	11.67	0.78	0.79
105	12.73	0.81	0.80
106	10.45	0.93	0.72

Table 2. 2015 disdrometer deployment summary. Probes with detected hail are shown and parent thunderstorms are denoted by the "In Operation" (IOP number) day and alphabetical label (i.e. IOP/Cell). Kinetic energies are subject to a maximum error of  $\pm 1.5$  J. Hail sizes are estimates and subject to error, especially in wind driven conditions. Total concentration represents accumulated number of impacts (probe surface area is 1 ft<sup>2</sup>).

Probe	ID	Location (km)	Maximum detected KE (J)	Mean detected KE (J)	Median detected KE (J)	Max size detected (cm)	Mean size detected (cm)	Total concentration (impacts ft <sup>2</sup> )
101	1/A	16 NW Vernon, TX	1.78	0.52	0.94	2.67	1.98	38
102	1/A	13 NW Vernon, TX	4.26	1.25	1.92	3.05	1.87	71
104	2/A	17 SW Woodson, TX	1.82	0.62	0.70	2.79	1.67	12
104	3/A	17 NW Childress, TX	0.65	0.19	0.35	1.78	1.54	7
105*	3/A	14 NW Childress, TX	7.88	1.65	3.85	3.56	1.87	206
104	3/B	3 S Dickens, TX	0.95	0.74	0.35	1.98	1.69	3
105*	3/B	7 S Dickens, TX	4.23	1.04	2.05	2.94	1.73	164
106	3/B	10 S Dickens, TX	17.95	8.46	10.3	4.85	1.97	74
103*	4/A	1 S Bucklin, KS	3.26	0.36	6.20	3.20	0.98	451
101	4/A	1 NW Bucklin, KS	2.51	0.93	2.41	3.04	2.10	189

\*possible detection of large drops (< 1 cm particles)

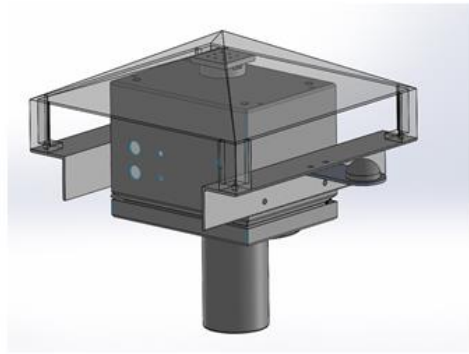
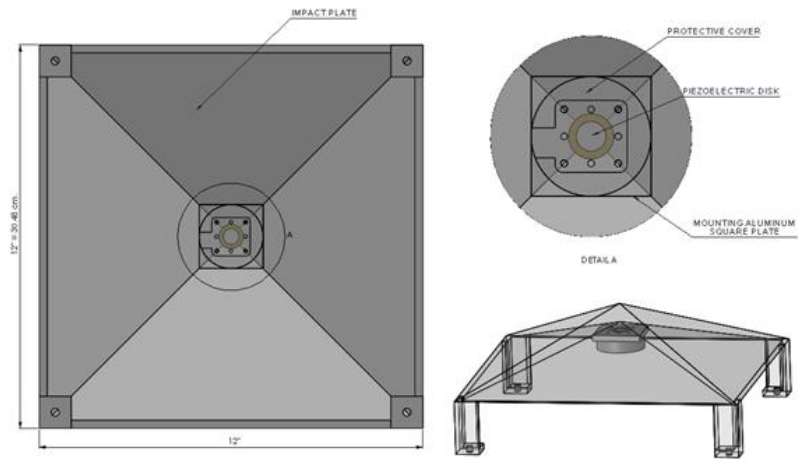


Figure 1. Diagram of disdrometer impact plate and components.



Figure 2. Photograph of the integrated Arduino Due and shield containing a microSD and GPS modules.

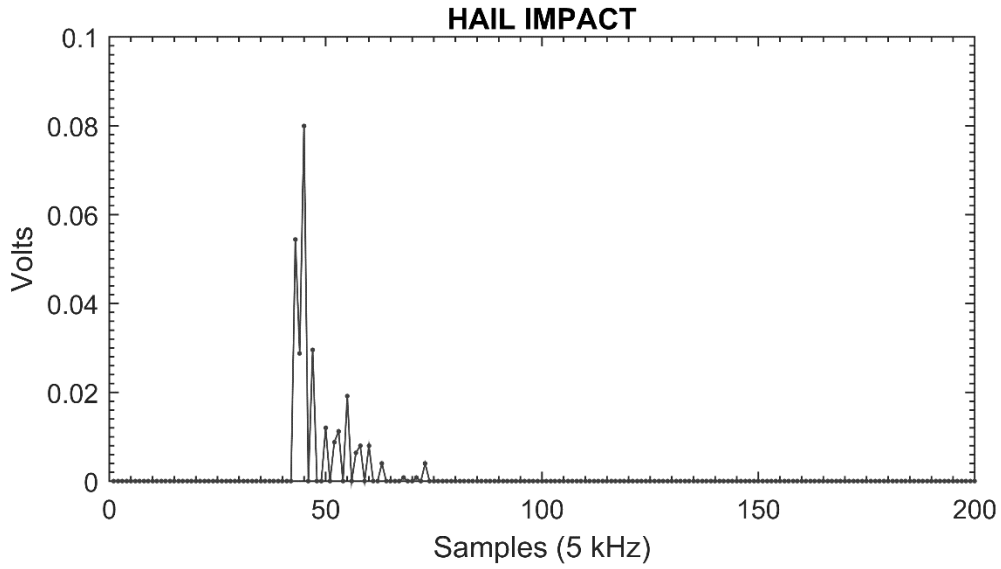


Figure 3. 5 KHz voltage time history on an actual hail impact captured by the system.

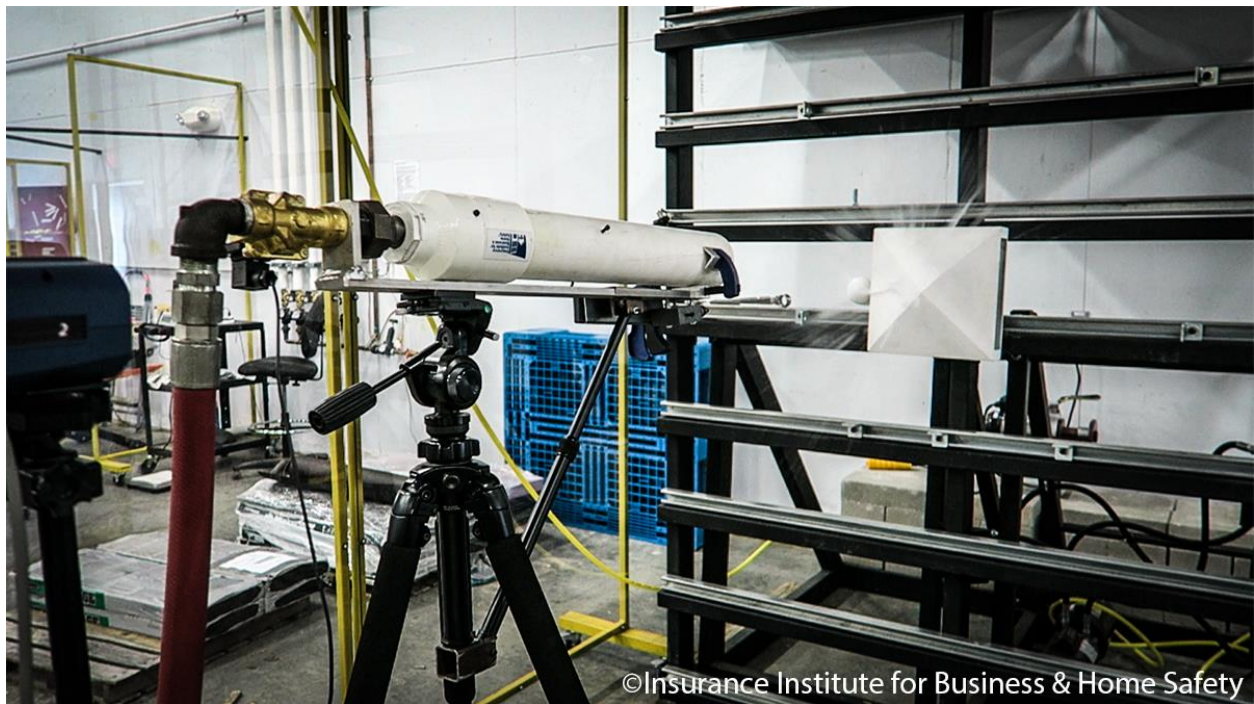


Figure 4. Photograph of a calibration ice sphere impact on Probe 101.

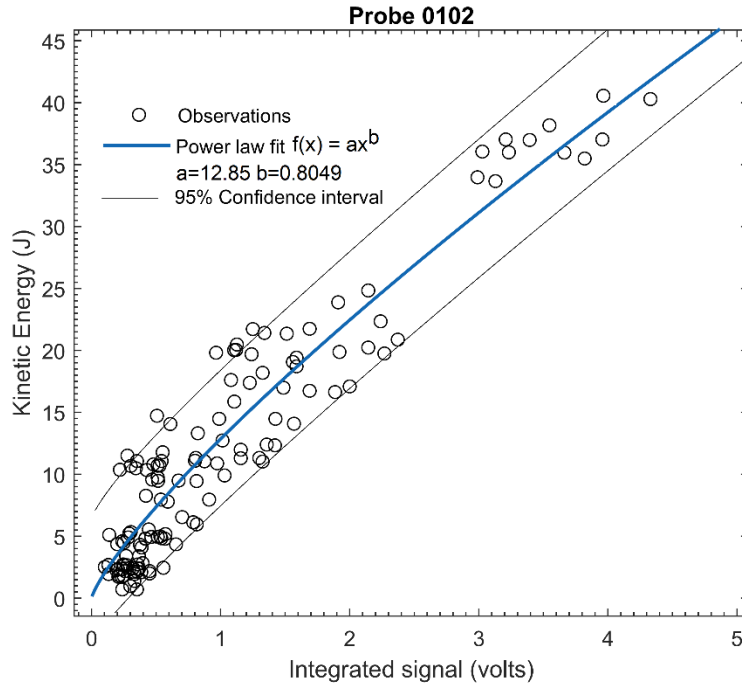


Figure 5. Calibration curve for Probe 102 showing the kinetic energy (measured) as a function of the area under the signal packet curve.

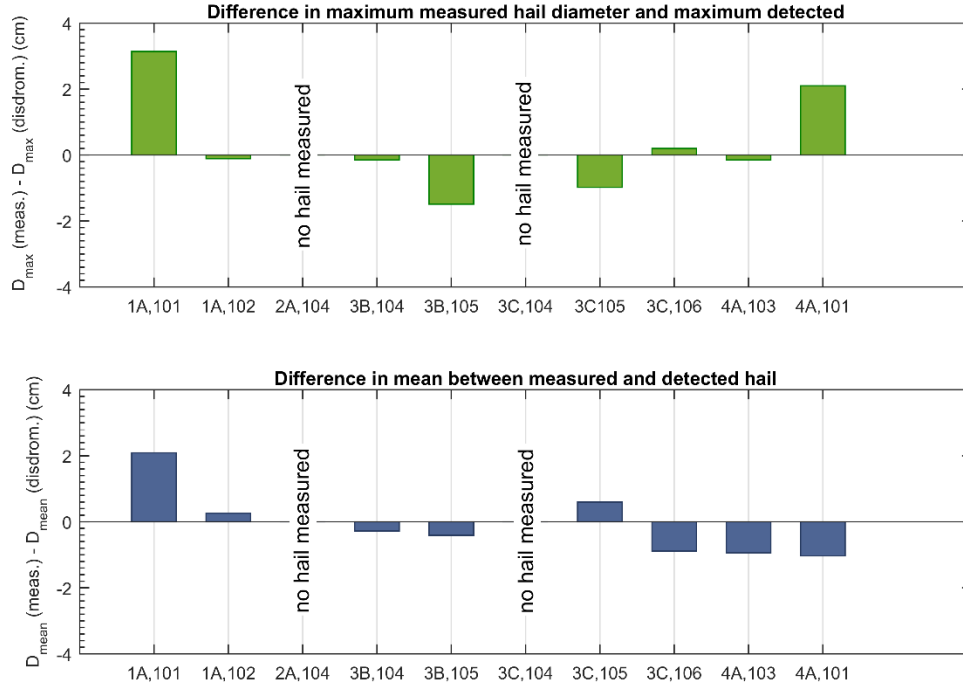


Figure 6. Difference between (top) maximum hail diameter measured and that detected by the disdrometer probe and (bottom) the difference between the mean hailstone diameter measured and the mean detected by the disdrometer probe. See Table 2 for deployment ID and IOP/Cell numbers.

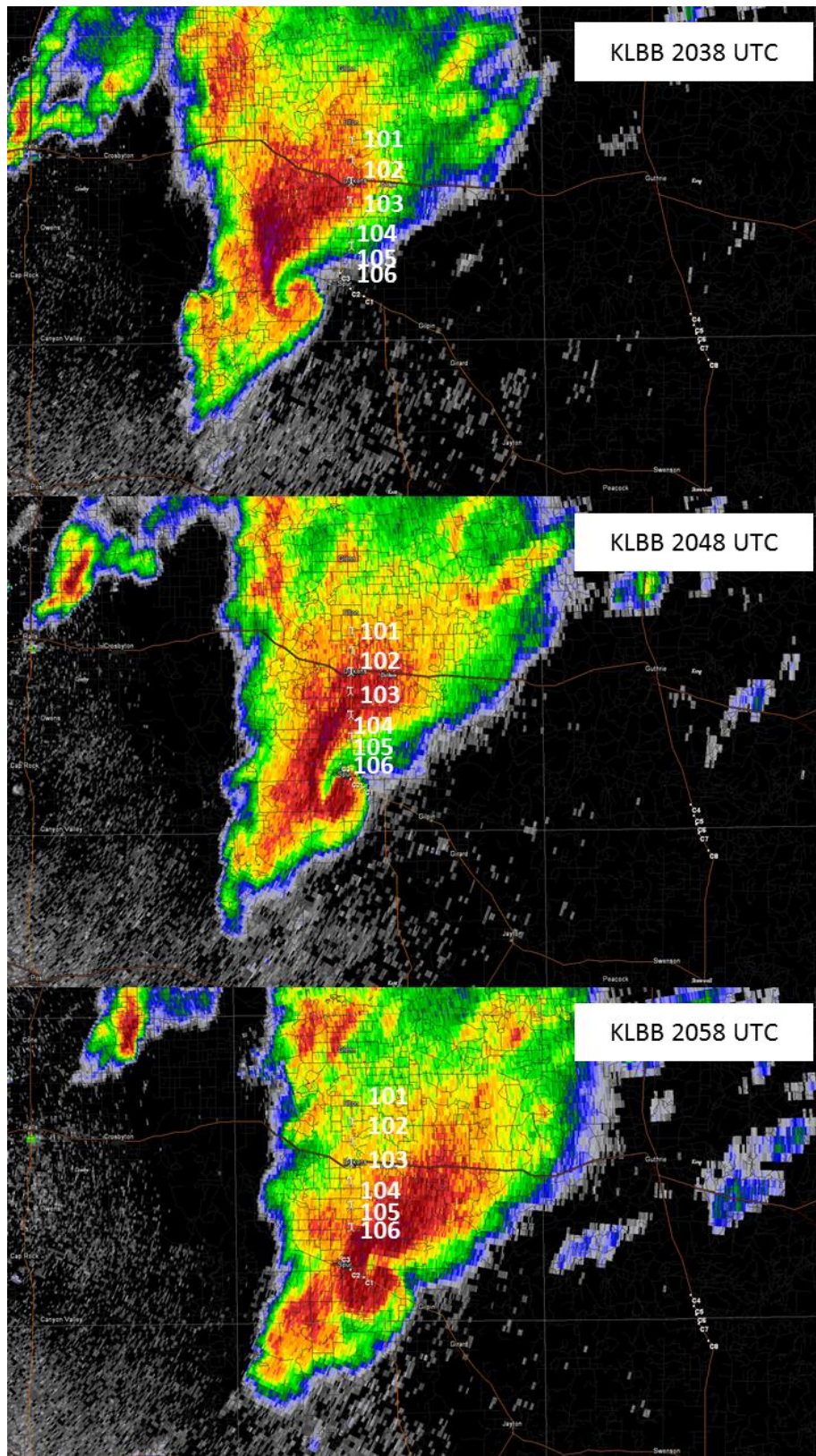


Figure 7. KLBB 0.5° horizontal reflectivity at (top) 2038 UTC, (middle) 2048 UTC, and (bottom) 2058 UTC on 8 May 2015. Probe locations are labeled.

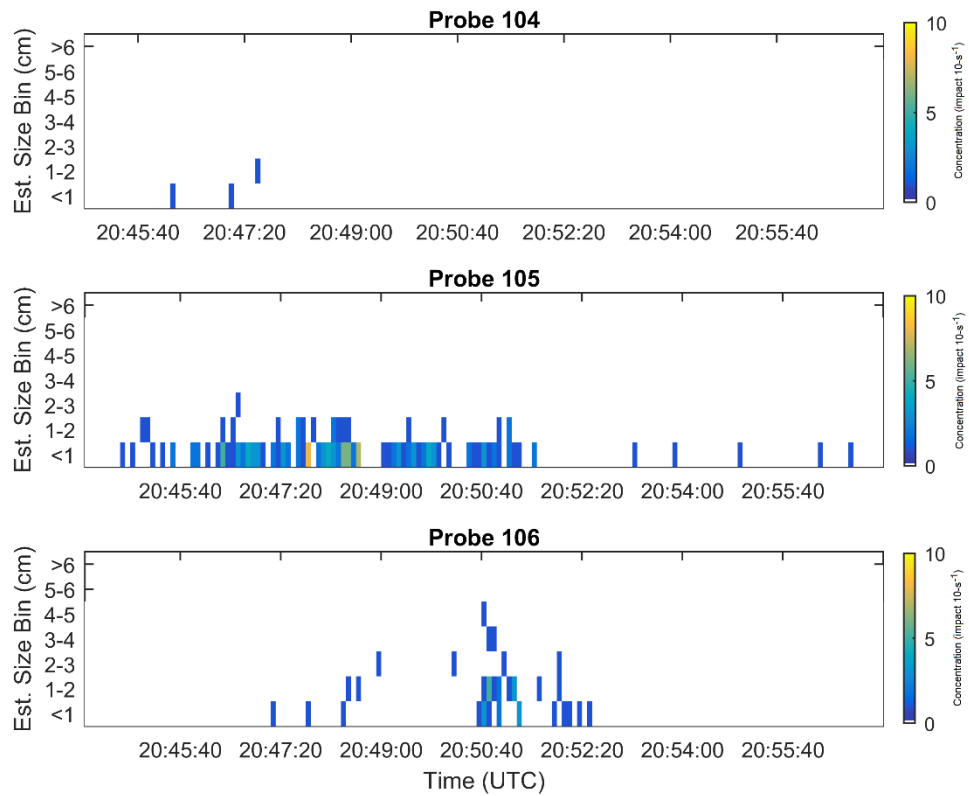


Figure 8. Time history of estimated hail size concentrations for (top) Probe 104, (middle) Probe 105, and (bottom) Probe 106 on 8 May 2016 for parent thunderstorm 3B (see Table 2). Hail sizes are grouped into 1 cm bins. The concentration represents the number of impacts on the disdrometer within the 10-second time window.